Laser and electrical current induced phase transformation of In$_2$Se$_3$ semiconductor thin film on Si(111)

**Chih-Yuan Lu · Patrick J. Shamberger ·
Esmeralda N. Yitamben · Kenneth M. Beck ·
Alan G. Joly · Marjorie A. Olmstead · Fumio S. Ohuchi**

Abstract Phase transformation of thin film ($\sim$30 nm) In$_2$Se$_3$/Si(111) (amorphous $\rightarrow$ crystalline) was performed by resistive annealing and the reverse transformation (crystalline $\rightarrow$ amorphous) was performed by nanosecond laser annealing. As an intrinsic-vacancy, binary chalcogenide semiconductor, In$_2$Se$_3$ is of interest for non-volatile phase-change memory. Amorphous In$_x$Se$_y$ was deposited at room temperature on Si(111) after pre-deposition of a crystalline In$_2$Se$_3$ buffer layer (0.64 nm). Upon resistive annealing to 380°C, the film was transformed into a γ-In$_2$Se$_3$ single crystal with its {0001} planes parallel to the Si(111) substrate and (11$\bar{2}$0) parallel to Si(1$\bar{1}$0), as evidenced by scanning tunneling microscopy, low energy electron diffraction, and X-ray diffraction. Laser annealing with 20-ns pulses (0.1 millijoules/pulse, fluence $\leq$ 50 mJ/cm^2) re-amorphized the region exposed to the laser beam, as observed with photoemission electron microscopy (PEEM). The amorphous phase in PEEM appears dark, likely due to abundant defect levels inhibiting electron emission from the amorphous In$_x$Se$_y$ film.

C.-Y. Lu
Intel Corporation, 5200 NE Elam Young Parkway, Hillsboro, OR 97124, USA

P.J. Shamberger · F.S. Ohuchi
Department of Materials Science and Engineering, University of Washington, Seattle, WA 98195-2120, USA

E.N. Yitamben · M.A. Olmstead
Department of Physics, University of Washington, Seattle, WA 98195-1560, USA

K.M. Beck (✉)
W.R. Wiley Environmental Molecular Sciences Laboratory, Pacific Northwest National Laboratory, PO Box 999 K8-88, Richland, WA 99352, USA
e-mail: kenneth.beck@pnl.gov

A.G. Joly
Fundamental and Computational Sciences, Pacific Northwest National Laboratory, PO Box 999 K8-88, Richland, WA 99352, USA

1 Introduction

Materials with rapid and reversible switching between their amorphous and crystalline phases, and which exhibit significant electrical resistivity and/or optical reflectivity change between these phases, are promising candidates for phase-change non-volatile memory. The strong change in optical reflectivity during the amorphous–crystalline phase transition in ternary chalcogenides is the basis of rewriteable compact disk and digital video disk technology, with Ge$_2$Sb$_2$Te$_5$ (GST) as the most commonly used material [1]. Over the past decade, binary chalcogenide semiconductors such as InSe/GaSe and In$_2$Se$_3$ have been investigated as potential phase-change media in proposed data storage and memory devices [2–4]. The electrical resistivity of In$_2$Se$_3$ increases by a factor of 10^5 from the crystalline to the amorphous state [3, 4], about 100 times larger than the resistivity change in GST [3]. However, the structural details of phase change in In$_2$Se$_3$ films on Si and the energetic requirements for phase change have not been fully explored.

In$_2$Se$_3$ exhibits a complex phase system in which various structures with different arrangements of inherent defects can form, in contrast to the simpler phase systems of Al$_2$Se$_3$ and Ga$_2$Se$_3$ [5, 6]. This complexity originates from many energetically similar routes by which trivalent

and divalent atoms can combine to satisfy their bonding requirements, and leads to several crystalline phases with the same In_2Se_3 stoichiometry (α, β, γ, δ, and κ) [7, 8]. This paper reports on the crystallization and amorphization of In_2Se_3 thin films on Si(111) ($\sim$30-nm thick) via resistive and laser annealing, respectively. The initially amorphous films were crystallized using resistive heating (time scale of several seconds), while a 150-micron-diameter spot was re-amorphized using nanosecond laser annealing. The film morphology and conductivity were probed with scanning tunneling microscopy (STM) and photoelectron emission microscopy (PEEM), the crystallinity with X-ray diffraction (XRD) and low energy electron diffraction (LEED), and the stoichiometry with Rutherford backscattering spectroscopy (RBS). The stoichiometry, morphology, and crystal structure of the crystallized In_2Se_3 film and its orientation with respect to the substrate are determined.

2 Experimental details

Experiments were carried out both at the Pacific Northwest National Laboratory, for PEEM and RBS, and at the University of Washington, Seattle, for ultra-high-vacuum (UHV) STM and LEED and ex situ two-dimensional X-ray diffraction (2D XRD). The film was grown and crystallized in Seattle under UHV and then transferred in atmosphere for 2D XRD, RBS, and PEEM.

Silicon substrates were cut from commercial p-type Si(111) wafers ($\rho \sim 1$ Ω cm) and prepared by repeated annealing of a chemically etched [9], outgassed sample to 1100°C for 5–10 s, followed by 20 min at 800°C and then a slow cool to room temperature to obtain a low-defect 7×7 reconstruction. Samples were heated by a direct current; the temperature was monitored using an optical pyrometer. Indium selenide was evaporated from In_2Se_3 granules (purity 99.999%) heated in a PBN crucible to temperatures between 900 and 1000°C, yielding a flux of 2–5 Å/min, as measured by a quartz crystal microbalance (QCM). An epitaxial In_2Se_3 layer of two bilayers (6.4 Å) was deposited on the Si(111) substrate at 555°C to serve as a buffer layer prior to amorphous film deposition. Other experiments have shown that this reduces the temperature needed to crystallize the film, as well as increasing its crystallinity [10], The amorphous In_xSe_y film was deposited atop the buffer layer at room temperature and subsequently annealed for crystallization (via electrical current through the substrate). The nominal deposition thickness of the film for which data are shown in Figs. 1, 2 and 3 was 47 nm (flux measured before growth on QCM $\times$ total deposition time); after annealing, RBS showed the film to be 27.5-nm thick. X-ray diffraction was performed on a Bruker D-8 diffractometer, with
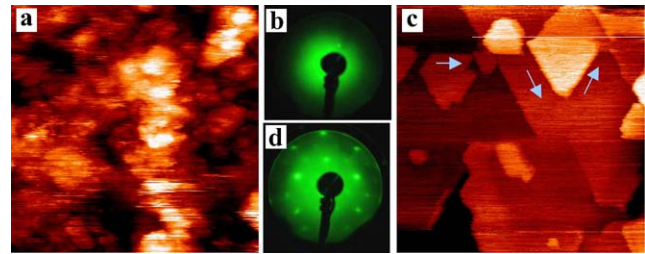

Fig. 1 Scanning tunneling microscopy (**a**, **c**, 200×200 nm^2) and low energy electron diffraction (**b**, **d**) of In_2Se_3/Si(111) deposited at room temperature on a crystalline In_2Se_3 buffer layer before (**a**, **b**) and after (**c**, **d**) annealing to 380°C. (**a**) STM of an as-deposited film (-10 V, 0.2 nA, color z scale 0–5 nm); (**b**) LEED pattern of the surface at electron energy $E_{el} = 47$ eV; (**c**) STM of the same film, imaged at 380°C (-9.8 V, 0.13 nA, color z scale 0–1.2 nm); (**d**) room temperature LEED pattern at electron energy $E_{el} = 47$ eV after annealing to 380°C

the incident Cu K_α excitation passing through a single Göbel mirror and a 0.5 mm pinhole collimator. Diffracted radiation was captured with a multiwire area detector. The beam was rastered across a sample area of 0.7 mm $\times$ 0.7 mm. The PEEM system was equipped with both Hg ($h\nu = 5.1$ eV) and D$_2$ ($h\nu = 6.0$ eV) sources for imaging a 150-μm-diameter region of the sample. A quadrupled Nd:YAG laser ($\lambda = 266$ nm, $h\nu = 4.7$ eV, FWHM pulse width 20 ns, spot diameter 100 μm, 0.1 mJ/pulse at 1-Hz repetition rate), incident through a UV-grade fused-silica window, was used to amorphize the crystalline film in situ.

3 Results

Figure 1 shows STM and LEED of a In_2Se_3/Si(111) film before (Fig. 1a and b) and after (Fig. 1c and d) resistive heating to 380°C. The morphology in Fig. 1a shows no distinctive structures, with an rms roughness of 1.2 nm on a 100×100 nm^2 area, showing that the film exhibits no nanoscale surface crystallinity. LEED (Fig. 1b) likewise shows no long-range order. The sample was then slowly heated in the STM chamber during continuous scanning until crystallization was observed. The amorphous In_xSe_y film fully crystallized at 380°C, well below the melting temperature. The image in Fig. 1c was taken at 380°C. The post-annealed morphology (Fig. 1c) shows that the edges of In_2Se_3 terraces and the edges of triangular overlayer islands on the terraces (height 0.32 nm) are aligned with directions of Si(111) (arrows); the rms roughness was 0.14 nm on a 100×100 nm^2 area. Subsequent, room temperature LEED patterns exhibited both 1×1 and $(\sqrt{3} \times \sqrt{3})$R30° spots (Fig. 1d).

The composition and thickness of the post-annealed In_xSe_y film were measured by Rutherford backscattering. In Fig. 2a, the dotted line is the experimental data and the solid line is a fit for a 2 to 3 ratio of In to Se (held fixed)
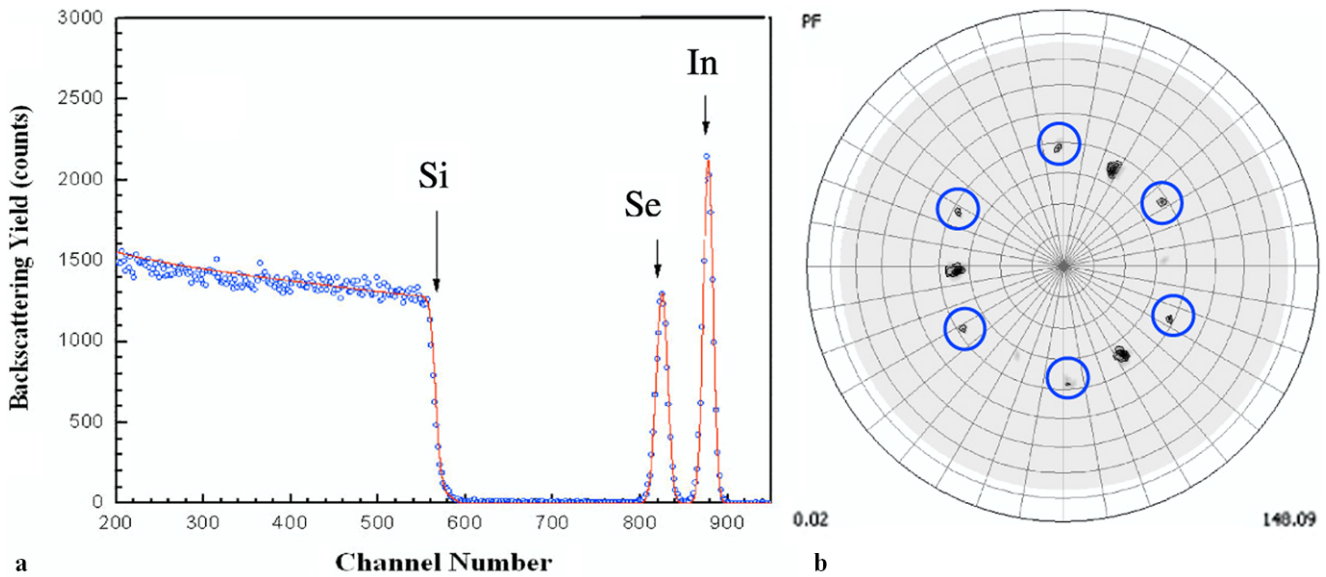
Fig. 2 (**a**) Rutherford backscattering spectrum (*dots*) of the phase-change In₂Se₃ thin film shown in Fig. 1, after annealing to 380°C. The *solid line* shows a fit to In:Se = 2:3 and thickness = 27.5 nm. (**b**) Pole figure showing six-fold symmetry of the γ-In₂Se₃(0001) film and three-fold symmetry of the underlying Si(111) substrate. $2\theta = 46.9$–$48.3°$ [Si(220) at 35° and γ-In₂Se₃($20\bar{2}8$) at 38°]

Fig. 3 PEEM images (field of view 150 μm, (*yellow*) scale bar 30 μm) for (**a**) clean Si(111); (**b**) an amorphous In₂Se₃ film on Si(111); (**c**) annealed In₂Se₃/Si(111) (same film as in Figs. 1 and 2); (**d**) after irradiation with 266-nm photon pulse. Images presented here are acquired with Hg lamp illumination ($h\nu = 5.1$ eV)
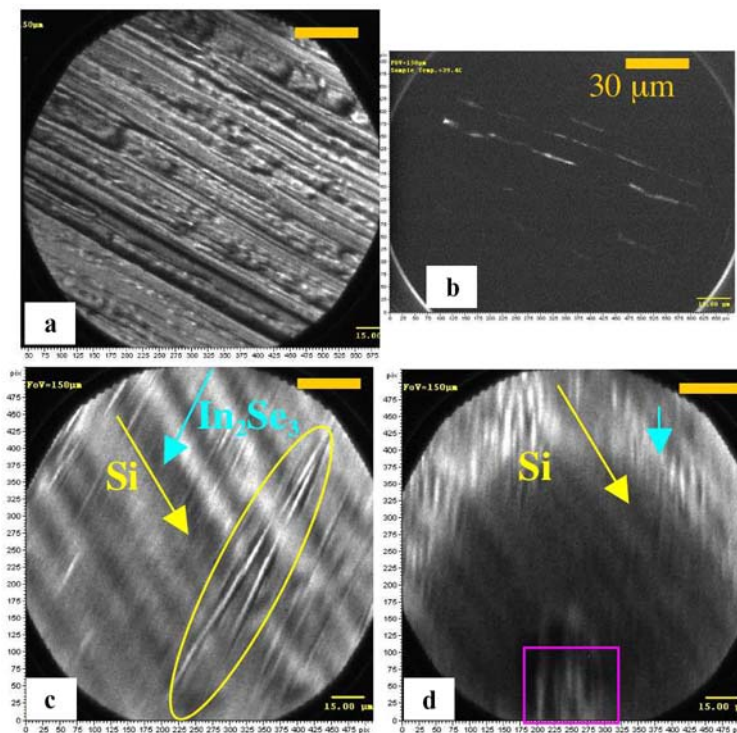
and a thickness of 27.5 nm (varied in the fit). The minimum yield (χ_{min}) value is 40%.

The 2D XRD measurements show that the annealed γ-In₂Se₃ film, which is clearly oriented on a 200-nm length scale in Fig. 1b, is predominantly a single crystal over a millimeter length scale. Other measurements without the crystalline buffer layer showed polycrystalline γ-In₂Se₃ after annealing [10]. The only In$_x$Se$_y$ phase observed for the film shown in Figs. 1 and 2 was γ-In₂Se₃ with fully relaxed lattice parameters: the (0006) peak at $2\theta = 27.65°$ ($d_{0006} = 3.23$ Å), (000 12) at $2\theta = 56.97°$ ($d_{00012} = 1.61$ Å), and ($10\bar{1}8$) at $2\theta = 40.0°$ ($d_{10\bar{1}8} = 2.25$ Å). A broad peak at $2\theta \sim 22.6°$ was also observed that may result from an oxide (e.g. In₂O₃ or In₂(SeO₄)₃). The in-plane texture align-

ment of the γ-In$_2$Se$_3$ film was probed via XRD pole figure measurements. The pole figure relative to the Si(111) surface normal for γ-In$_2$Se$_3$ (20$\bar{2}$8) is shown in Fig. 2b. The γ-In$_2$Se$_3$ (20$\bar{2}$8) planes have spacing $d_{20\bar{2}8} = 1.90$ Å and make an angle of 38° towards [10$\bar{1}$0] with γ-In$_2$Se$_3$ (0001), while Si(220) planes have spacing $d_{220} = 1.91$ Å and make an angle of 35° towards [11$\bar{2}$] with Si(111). Because of the similarity in plane spacing, both peaks may be acquired in the same pole figure. The three-fold-symmetric spots in Fig. 2b are thus attributed to the Si substrate, while the six-fold pattern is from well-oriented γ-In$_2$Se$_3$ (20$\bar{2}$8). The 30° rotation between the Si(220) and γ-In$_2$Se$_3$ scattering shows that γ-In$_2$Se$_3$ [11$\bar{2}$0] is aligned with Si[1$\bar{1}$0].

While a slow anneal below the melting temperature can lead to crystallization of an amorphous film, returning to the amorphous state requires rapid heating and cooling to quench in the disordered state. This was accomplished with pulsed laser annealing. The sample was monitored with photoelectron emission microscopy (PEEM), which distinguishes structures on the surface through a combination of their work function, electrical conductivity, and density of states near the Fermi level [11–13].

Figure 3a shows a PEEM image of a clean Si(111) substrate after being Ar sputtered and then annealed to ∼850°C. An amorphous In$_2$Se$_3$/Si(111) film deposited under similar conditions to those for the film in Figs. 1 and 2, but without a crystalline buffer layer, is shown in Fig. 3b. The room-temperature-deposited In$_2$Se$_3$ film presents a completely dark PEEM image with either Hg (5.1 eV) or D$_2$ (6.0 eV) illumination, except for defect lines running through the center of the image. The work function of In$_2$Se$_3$ is reported to be 4.35 eV [14], which should yield emission with either source. PEEM images of the same film as for Figs. 1 and 2 are shown before (Fig. 3c) and after (Fig. 3d) laser annealing. Similar results were obtained with both Hg and D$_2$ illumination, although only the Hg results are shown. Comparison to bare Si (Fig. 3a) indicates that the wider stripe structure running from upper left to lower right arises from the underlying Si terrace structure (yellow arrows), while the narrower lines (blue arrows) correspond to the texture of the In$_2$Se$_3$ films. Two crossed lines marked in the oval are defects on the surface. The 266-nm laser was used to anneal a spot on the sample approximately 150 microns in diameter near the place where the image in Fig. 3c was taken. Single pulses of 0.1 mJ and 20-ns duration were measured at the laser head. Subsequent aperture reduction and focusing culminated in a final pulse fluence of <50 mJ/cm^2. The resulting annealed region is shown in Fig. 3d, where a dark circular region may be observed surrounded by features characteristic of the crystalline In$_2$Se$_3$ film. The darker region still shows (though with less contrast) the structure characteristic of the underlying Si substrate, with In$_2$Se$_3$ features less distinct.

4 Discussion

Room-temperature deposition of In$_2$Se$_3$ on Si(111) results in an amorphous film, even when a crystalline template is first deposited. The nominal thickness from the crystal monitor was over 40% larger than that measured with RBS after annealing. The In:Se ratio measured by RBS after annealing (2:3) was equal to that in the incident deposition flux, indicating that any evaporation must have been congruent. However, rather than re-evaporation at 380°C, it is more likely either that the flux decreased during deposition or that the geometry was slightly different from when the QCM was calibrated. The rms height variation on a 100×100 nm^2 area is reduced from 1.2 nm to 0.14 nm ($\sim$1 bilayer) upon annealing. On similar 100×100 nm^2 areas, the original Si(111) substrate had an rms roughness of 0.37 nm, while the crystalline buffer layer (0.7-nm thick) had an rms roughness of 0.23 nm. After further annealing than the images in Fig. 1, the surface showed 8-nm-deep triangular pits with a density $\sim$10 per square micron, and 0.22 nm rms roughness between the pits. There are several known crystal structures of In$_2$Se$_3$, each with a different arrangement of the intrinsic vacancies. α-In$_2$Se$_3$ has a layered hexagonal structure with $a = 4.03$ Å and $c = 19$ Å. Each layer is built up from tetrahedral covalent bonds in the sequence Se–In–Se–In–Se (a penta layer) along the c axis [15], and the In vacancies are localized in (0001) planes. The β phase is also hexagonal ($a = 4.03$ Å and $c = 28$ Å) and metastable. It can be obtained by heating α-In$_2$Se$_3$ to 523 K [16]. γ-In$_2$Se$_3$ is the stable room temperature phase, a defected wurtzite structure with $a = 7.13$ Å and $c = 19.38$ Å [7, 17, 18]. The unit cell of γ-In$_2$Se$_3$ contains six bilayers. Each In layer has vacancies arranged in a $(\sqrt{3} \times \sqrt{3})$R30° pattern, with a helical alignment from layer to layer [7, 17, 18]. The δ phase exists at very high temperature (973 K) and could be a product of dissociation of In$_2$Se$_3$. A new phase, κ-In$_2$Se$_3$, with the unit-cell symmetry similar to α-In$_2$Se$_3$ was recently discovered, with Zn doping necessary to obtain and stabilize κ-In$_2$Se$_3$ thin films at room temperature [19, 20].

Annealing amorphous In$_2$Se$_3$/Si resulted in formation of single-crystal γ-In$_2$Se$_3$, which is supported by LEED, STM, and XRD. The hexagonal 1×1 LEED spots would arise from the (oriented) hexagonal lattice in 0001 planes of any wurtzite-based phase of In$_2$Se$_3$, but the $(\sqrt{3} \times \sqrt{3})$R30° spots are consistent with intrinsic vacancy ordering in γ-In$_2$Se$_3$ continuing to the surface. α-In$_2$Se$_3$, in contrast, has no reason for surface reconstruction, since the (0001) planes between penta layers have no dangling bonds. The LEED is thus excellent evidence for long-range order in the intrinsic vacancies, and shows that the surface of the 30-nm-thick film is still oriented relative to the underlying Si substrate. The STM data show this oriented alignment as well, with the step edges of the In$_2$Se$_3$ film well aligned with those of

the underlying substrate. The STM step height of 0.32 nm is also consistent with the γ phase (it would be 0.95 nm in the α phase). The XRD data further confirms the assignment of single-crystal γ-In$_2$Se$_3$. The plane spacings are slightly larger in the γ phase than in the α phase. The off-axis planes such as $(20\bar{2}8)$, $(10\bar{1}8)$, and $(11(\bar{2})6)$ that we observe would also be at slightly different orientation angles and 2θ values. The pole figure in Fig. 2b clearly shows the relative orientation of the Si and γ-In$_2$Se$_3$ lattices. The Si(220) spots lie in an azimuth 30 from γ-In$_2$Se$_3$$(20\bar{2}8)$. Note that the underlying wurtzite lattice is not rotated relative to the diamond structure, however, since the $(\sqrt{3} \times \sqrt{3})$R30° vacancy ordering that determines the γ-In$_2$Se$_3$ unit cell yields unit vectors rotated 30° from those of the underlying wurtzite structure. The crystallization process of amorphous In$_2$Se$_3$ occurs at a temperature well below the melting temperature [21], and also occurs at a lower temperature (380°C) when a crystalline buffer layer is deposited before the amorphous layer than when the film is deposited directly on Si(111) at room temperature (450°C for a 17-nm thick film). Annealing the pure amorphous film resulted in a polycrystalline film, with random in-plane orientation, although the (0001) axis was still normal to the film [10].

The inverse process of amorphization likely requires local melting of the In$_2$Se$_3$. An order of magnitude estimate of the energy required for amorphization is $3Nk_b \times 1000$ K, [m.p. = 1158 K, γ-In$_2$Se$_3$], where N is the number of atoms in the heated volume and k_b is Boltzmann's constant. The volume of film exposed to the laser (27.5-nm thick, 100-μm diameter) had about 7×10^{13} atoms, for which $3Nk_b \times 1000$ K is about 3 μJ, or about 1/30 the energy in each laser pulse. Since the absorption length of the 266-nm radiation is 10–100 nm ($\alpha \sim 10^5$–10^6 cm^{-1}) [16], some of the energy is deposited in the substrate; additional energy is also lost to the optics. It is thus not surprising that a few pulses were required to initially heat the area before a single pulse would carry a region over threshold for amorphization. The contrast between the crystalline and amorphous regions in PEEM could arise from differences in work function, in densities of states near the Fermi level, or in film conductivity. The work function of crystalline In$_2$Se$_3$ is 4.35 eV [14], so both Hg (5.1 eV) and D$_2$ (6.0 eV) illumination should result in electron emission. Our photoemission measurements on a 1-nm-thick film [10] show an In $4d$ core level shift of $\sim$0.7 eV to higher binding energy (relative to the Fermi energy) from the amorphous to the annealed phase. If the In shift were completely due to a change in work function, then the Hg radiation would be close to threshold for photoemission, but there should still be significant emission with D$_2$ radiation. However, we find no emission with either source for the as-deposited film except at large-scale defects (Fig. 3b). It is thus likely that photoexcited electrons become trapped in the amorphous material and cannot

travel to the surface for emission into vacuum. The laser-amorphized film (Fig. 3d) still shows a small amount of emission, mostly from the underlying Si substrate, indicating that it has fewer trapping defects than the as-deposited film, but still no states that can emit electrons. Upon returning to the same point on the sample as in Fig. 3c, the defect in the oval greatly increased in relative intensity, becoming twice as bright as its surroundings. This indicates impact of the laser beam through heating and/or free-carrier excitation in the substrate over a range of a few hundred microns.

5 Conclusions

The control of material phase (amorphous, or one of several possible crystalline or polycrystalline states) is essential to the properties of modern devices. The difference in properties associated with a phase change may be exploited for device operations, as in DVDs where the change in optical reflectivity between crystalline and amorphous states allows media rendition. Driven by the need for a new paradigm to continue the relentless increase in both density and speed that has characterized developments in computer memory for four decades, one promising avenue for non-volatile memory is phase-change memory (PCM), for which chalcogenides are prime candidates. Amorphous–crystalline phase transitions can be achieved by applying voltage pulses with different amplitudes and durations in the range of tenths of nanoseconds. In our study, we have shown that rapid, selective, and local crystalline–amorphous transformation can be realized using pulsed, UV nanosecond lasers at low fluences. This is a necessary step in the development of high-density/high-speed chalcogenide-based optical PCM.

References

1. T. Ohta, J. Optoelectron. Adv. Mater. **3**, 609 (2001)
2. A. Chaiken, G.A. Gibson, J. Chen, B.S. Yeh, J.B. Jasinski, Z. Liliental-Weber, K. Nauka, C.C. Yang, D.D. Lindig, S. Subramanian, Jpn. J. Appl. Phys. **45**, 2580 (2006)
3. H. Lee, Y.K. Kim, D. Kim, D.-H. Kang, IEEE Trans. Magn. **41**, 1034 (2005)

4. H. Lee, D.-H. Kang, L. Tran, Mater. Sci. Eng. B **119**, 196 (2005)
5. Landolt-Bornstein, *Group IV Physical Chemistry—Phase Equilibria, Crystallographic and Thermodynamic Data of Binary Alloys*, vol. 5A
6. Landolt-Bornstein, *Group IV Physical Chemistry—Phase Equilibria, Crystallographic and Thermodynamic Data of Binary Alloys*, vol. 5F
7. J. Ye, S. Soeda, Y. Nakamura, O. Nittono, Jpn. J. Appl. Phys. **37**, 4264 (1998)
8. C. Amory, J.C. Bernede, S. Marsillac, J. Appl. Phys. **94**, 6945 (2003)
9. A. Ishizaka, Y. Shiraki, J. Electrochem. Soc. **133**, 666 (1986)
10. C.-Y. Lu, PhD dissertation, University of Washington, 2007
11. M. Giesen, R.J. Phaneuf, E.D. Williams, T.L. Einstein, H. Ibach, Appl. Phys. A **64**, 423 (1997)
12. A. Gloskovskii, D. Valdaitsev, S.A. Nepijko, N.N. Sedov, G. Schonhense, Appl. Phys. A **79**, 707 (2004)
13. W.Y. Li, K. Goto, R. Shimizu, Surf. Interface Anal. **37**, 244 (2005)
14. S. Sakalauskas, A. Sodeika, Rev. Sci. Instrum. **69**, 166 (1998)
15. M. Ishikawa, T. Nakayama, Jpn. J. Phys. **36**, L1576 (1997)
16. H.T. El-Shair, A.E. Bekheet, J. Phys. D **25**, 1122 (1992)
17. A. Likforman, D. Carré, Acta Crystallogr. B **34**, 1 (1978)
18. J. Ye, T. Yoshida, Y. Nakamura, O. Nittono, Appl. Phys. Lett. **67**, 3066 (1995)
19. C. de Groot, J.S. Moodera, J. Appl. Phys. **89**, 4336 (2001)
20. J. Jasinky, W. Swider, J. Washburn, Z. Liliental-Weber, A. Chaiken, K. Nauka, G.A. Gibson, C.C. Yang, Appl. Phys. Lett. **81**, 4356 (2002)
21. Landolt-Bornstein, *Group IV Physical Chemistry—Phase Equilibria, Crystallographic and Thermodynamic Data of Binary Alloys*, vol. 5G